A sliding coherence window technique for hierarchical detection of continuous gravitational waves

Holger J. Pletsch[*]

Max-Planck-Institut für Gravitationsphysik (Albert-Einstein-Institut) and
Leibniz Universität Hannover, Callinstraße 38, D-30167 Hannover, Germany
(Dated: 02:32, Monday 31$^{\text{st}}$ January, 2011)

A novel hierarchical semicoherent technique is presented for all-sky surveys for continuous gravitational-wave sources, such as rapidly spinning non-axisymmetric neutron stars. Analyzing year-long detector data sets over realistic ranges of parameter space using fully-coherent matched-filtering is computationally prohibitive. Thus more efficient, so-called hierarchical techniques are essential. Traditionally, the standard hierarchical approach consists of dividing the data into non-overlapping segments of which each is coherently analyzed and subsequently the matched-filter outputs from all segments are combined incoherently. The present work proposes to break the data into subsegments being shorter than the desired maximum coherence time span (size of the coherence window). Then matched-filter outputs from the different subsegments are efficiently combined by "sliding" the coherence window in time: Subsegments whose time-stamps are closer than coherence window size are combined coherently, otherwise incoherently. Compared to the standard scheme at the same coherence time baseline, data sets longer by about $50\,\% - 100\,\%$ would have to be analyzed to achieve the same search sensitivity as with the sliding coherence window approach. Numerical simulations attest the analytically estimated improvement.

PACS numbers: 04.80.Nn, 95.55.Ym, 95.75.-z, 97.60.Gb

I. INTRODUCTION

Rapidly rotating neutron stars are anticipated to emit continuous gravitational-wave (CW) signals through various plausible scenarios [1–6] due to asymmetries. While the majority of such neutron stars eludes electromagnetic observations, their population might potentially only be probed by means of gravitational waves. Currently an international network of laser-interferometric detectors [7–10] is in operation and numerous CW search efforts have been undertaken [11–15]. The observational upper limits obained so far already constrain the physics of neutron stars [13, 16, 17] and thus a detection of a CW signal from a spinning neutron star would shed light on their currently rather uncertain physics [18].

Extremely sensitive data analysis techniques are needed to detect CW signals because of their expected low signal-to-noise ratios. A powerful method has been derived [19] based on the principle of maximum likelihood detection, leading to coherent matched filtering. CW signals are quasimonochromatic with a slowly changing intrinsic frequency. However, the Earth's motion relative to the solar system barycenter (SSB) generates a Doppler modulation in amplitude and phase of the waveform at a terrestrial detector. As shown in [19], the coherent matched-filtering statistic can be analytically maximized over the *amplitude parameters* describing the signal's amplitude variation. The so-obtained coherent detection statistic is referred to as the $\mathcal{F}$-statistic, which can also include multiple detector data streams [20]. Thus, an explicit search (evaluating $\mathcal{F}$) is only done over the *phase parameters* describing the signal's phase evolution: the source's sky location, frequency, and frequency derivatives ("spindowns").

However, what ultimately limits the search sensitivity in scanning the entire sky for previously unknown CW sources is the finite computational resources. For year-long data sets, searching a realistic portion of parameter space is computationally absolutely impractical [19, 21]. This is due to the apparently enormous number of template waveforms needed to discretely cover the search parameter space, increasing as a high power of the coherent integration time. In consequence, viable all-sky fully-coherent $\mathcal{F}$-statistic searches are restricted to much shorter coherent integration times of order days, despite that the $\mathcal{F}$-statistic can be very efficiently computed using the fast Fourier transform (FFT) algorithm [19, 22].

To sift through year-long data sets at given computational constraints, more efficient, hierarchical methods have been developed [11, 23–28] . By the "standard" hierarchical semicoherent search strategy, this work refers to the following scheme. One breaks the data into non-overlapping segments of duration T, each of which is analyzed *coherently*, then all segments are *incoherently* combined. Therefore T defines the coherent time baseline (the maximum time span of coherent integration) and is typically of order days. The notion "semicoherent" stems from the fact that in this scheme phase information *between* coherent segments is discarded.

The hierarchical semicoherent search approach is efficient, because the coherent matched-filtering statistic $\mathcal{F}$ is just computed by integrating over each segment whose duration is much smaller than the entire data set. Hence a *coarse* grid of templates in phase parameter space can be used for every segment. Only when incoherently combining the $\mathcal{F}$ values from all segments a common *fine* grid of templates is necessary.

Recent progress in understanding the global correlations [29, 30] of the $\mathcal{F}$-statistic in the phase parameters has lead to a substantially more sensitive hierarchical semicoherent search technique [28]. This method has addressed a long-standing problem, namely the design of, and link between, the coarse and fine grids. A very useful geometric tool in this context is the concept of a metric, as first investigated in

---

[*]Electronic address: Holger.Pletsch@aei.mpg.de

[31, 32], measuring the fractional loss in expected $\mathcal{F}$-statistic for a given signal at a nearby grid point. While such a metric has been well studied for the coherent stage [21, 33, 34], in [28] the first analytical metric for the incoherent combination step has been found by exploiting new coordinates on the phase parameter space. This analytical "semicoherent metric" has lately been further studied and extended to greater generality in [35]. This technology is currently also implemented and employed by Einstein@Home [15], a volunteer distributed computing project carrying out the most sensitive all-sky CW surveys.

The present work presents a novel hierarchical semicoherent search strategy which builds on the results of [28, 35], further enhancing the search sensitivity. Previous hierarchical search methods divide the data into non-overlapping segments whose length is equal to coherent time baseline T. Here, a partitioning of the data into segments *shorter* than the desired maximum coherence length T is considered and subsequently one "slides" a coherence window of size T over the segments. As a result, segments which are closer than coherence window size T are coherently combined and otherwise incoherently. This scheme also ensures that the same semicoherent metric as derived in [28, 35] governs the template grid construction in phase parameter space, but considerably enhances the overall search sensitivity.

Section II briefly recaps the continuous gravitational-wave signal waveform. Section III B describes the coherent matched-filtering statistic $\mathcal{F}$ and the standard hierarchical search scheme. The idea behind the sliding coherence window approach is elucidated in Sec. IV, along with an analytical sensitivity estimation. The improved performance is demonstrated in Sec. V by means of Monte Carlo simulations. In addition, Sec. VI compares the sensitivity at fixed computational cost. Finally, concluding remarks follow in Sec. VII.

II. CONTINUOUS GRAVITATIONAL-WAVE SIGNALS

The dimensionless signal response function $h(t)$ of an interferometric detector to a weak plane gravitational wave in the long-wavelength approximation is a linear combination of the form [19],

$$h(t) = F_+(t)\, h_+(t) + F_\times(t)\, h_\times(t)\,. \qquad (1)$$

The antenna pattern functions $F_+(t)$ and $F_\times(t)$ are given by

$$F_+(t) = a(t)\cos 2\psi + b(t)\sin 2\psi\,, \qquad (2a)$$
$$F_\times(t) = b(t)\cos 2\psi - a(t)\sin 2\psi\,, \qquad (2b)$$

where ψ represents the polarization angle of the signal and the angle between the detector arms is assumed to be $\pi/2$. For explicit expressions of the functions $a(t)$ and $b(t)$ the reader is referred to Ref. [19].

In the case of an isolated, rapidly rotating neutron star with a non-axisymmetric deformation and negligible proper motion (cf. [36, 37]), the waveforms corresponding to the plus ($+$) and cross ($\times$) polarizations are

$$h_+(t) = A_+\sin\Psi(t)\,, \qquad h_\times(t) = A_\times\cos\Psi(t)\,, \qquad (3)$$

where A_+ and $A_\times$ are the constant plus and cross polarization amplitude parameters, respectively, and $\Psi(t)$ is the phase of the signal. The parameters A_+ and $A_\times$ can be expressed in terms of the gravitational-wave strain tensor amplitude h_0 and the inclination angle ι as

$$A_+ = h_0\left(1 + \cos^2\iota\right)/2\,, \qquad A_\times = h_0\cos\iota\,. \qquad (4)$$

The phase $\Psi(t)$ of the CW signal at detector time t takes the following form [19]:

$$\begin{aligned}\Psi(t) &= \Phi_0 + \Phi(t) \\ &= \Phi_0 + 2\pi\sum_{k=0}^{s}\frac{f^{(k)}(t_0)}{(k+1)!}\left[t - t_0 + \frac{\vec{r}(t)\cdot\vec{n}}{c}\right]^{k+1}\,, \end{aligned} \qquad (5)$$

where Φ_0 is the initial phase, $f^{(0)} \equiv f$ denotes the frequency, and $f^{(k>0)}$ is the kth frequency time derivative (also called "spindown"), evaluated at the SSB at time t_0. The integer $s > 0$ denotes the number of frequency time derivatives to be taken into account, therefore it holds $f^{(k>s)} = 0$. The vector $\vec{r}(t)$ connects from the SSB to the detector, c is the speed of light, and $\vec{n}$ is a constant unit vector pointing from the SSB to the location of the CW source. A source's sky location is determined by two independent coordinates, for example one can use equatorial coordinates of right ascension and declination, denoted by α and δ, respectively. In these coordinates: $\vec{n} = (\cos\delta\,\cos\alpha, \cos\delta\,\sin\alpha, \sin\delta)$. The collection of phase parameters will be summarized by the vector $\mathbf{p} \equiv \left(f, f^{(1)}, ..., f^{(s)}, \alpha, \delta\right)$.

Using Eqs. (2), (3) and (5), it is possible to rewrite Eq. (1) as follows

$$h(t) = \sum_{\mu=1}^{4}\mathcal{A}_\mu h_\mu(t)\,, \qquad (6)$$

where the four amplitude parameters $(A_+, A_\times, \psi, \Phi_0)$ have been reparameterized by the 4-vector $\mathcal{A} \equiv (\mathcal{A}_1, \mathcal{A}_2, \mathcal{A}_3, \mathcal{A}_4)$, whose individual components are

$$\mathcal{A}_1 = A_+\,\cos 2\psi\,\cos\Phi_0 - A_\times\sin 2\psi\,\sin\Phi_0\,,$$
$$\mathcal{A}_2 = A_+\,\sin 2\psi\,\cos\Phi_0 + A_\times\cos 2\psi\,\sin\Phi_0\,,$$
$$\mathcal{A}_3 = -A_+\,\cos 2\psi\,\sin\Phi_0 - A_\times\sin 2\psi\,\cos\Phi_0\,,$$
$$\mathcal{A}_4 = -A_+\,\sin 2\psi\,\sin\Phi_0 + A_\times\cos 2\psi\,\cos\Phi_0\,, \qquad (7)$$

and the functions $h_\mu(t)$ have been defined as

$$\begin{aligned} h_1(t) &= a(t)\cos\Phi(t)\,, \quad h_2(t) = b(t)\cos\Phi(t)\,, \\ h_3(t) &= a(t)\sin\Phi(t)\,, \quad h_4(t) = b(t)\sin\Phi(t)\,. \end{aligned} \qquad (8)$$

III. STANDARD HIERARCHICAL DETECTION SCHEME

At a given detector time t, the detector output data time series [52] is denoted by $x(t)$. In the absence of any signal, the data contain only noise $n(t)$, which is assumed to be a

zero-mean, stationary, and Gaussian random process. When a signal $h(t)$ is present, the noise is assumed to be additive, so that $x(t) = n(t) + h(t)$.

In the "standard" hierarchical semicoherent search scheme one divides the data into N *non-overlapping* segments. Each segment has duration T, the coherent time baseline. For simplicity the data set is taken to be contiguous, so that the total data time span is written as $T_{\mathrm{data}} = NT$. The individual segments are labeled by the index $j = 1, ..., N$. Thus, let t_j denote the time midpoint of segment j, that spans the interval $[t_j - T/2, t_j + T/2]$. Each of these segments is analyzed coherently, and in a second step, the matched-filtering outputs from all segments are incoherently combined. This is the standard scheme which will be further elucidated below.

A. Coherent matched-filtering of one segment

1. The $\mathcal{F}$-statistic

The likelihood ratio Λ_j for the jth segment, deciding between the hypothesis of a signal $h(t)$ with amplitude parameters $\mathcal{A}$ and phase parameters $\mathbf{p}$, and no signal being present, is written as [19],

$$\ln \Lambda_j = (x|h)_j - \frac{1}{2}(h|h)_j \,, \tag{9}$$

where the following inner product has been used [19],

$$(x|y)_j \equiv \frac{2}{S_n^{[j]}} \int_{t_j - T/2}^{t_j + T/2} x(t)\, y(t) \mathrm{d}t \,. \tag{10}$$

with $S_n^{[j]}$ defined as the one-sided noise spectral density for the jth segment. Since this work is concerned with narrow-bandwidth signals, $S_n^{[j]}$ is here taken as constant.

As done in Ref. [19], the following inner products are combined for every segment j into a 4×4 matrix $\mathcal{M}^{[j]}$ whose components are

$$\mathcal{M}_{\mu\nu}^{[j]} \equiv (h_\mu|h_\nu)_j \,, \tag{11}$$

where $\mu, \nu = 1, 2, 3, 4$. To very good accuracy, one can approximate [19],

$$(h_1|h_3)_j \approx (h_1|h_4)_j \approx (h_2|h_3)_j \approx (h_2|h_4)_j \approx 0 \,, \tag{12a}$$

$$(h_1|h_1)_j \approx (h_3|h_3)_j \approx \frac{1}{2}A_j \,, \tag{12b}$$

$$(h_2|h_2)_j \approx (h_4|h_4)_j \approx \frac{1}{2}B_j \,, \tag{12c}$$

$$(h_1|h_2)_j \approx (h_3|h_4)_j \approx \frac{1}{2}C_j \,, \tag{12d}$$

with the definitions

$$A_j \equiv (a|a)_j \,, \quad B_j \equiv (b|b)_j \,, \quad C_j \equiv (a|b)_j \,. \tag{13}$$

In addition we abbreviate the linear correlations $(x|h_\mu)_j$ by the following compact notation,

$$x_\mu^{[j]} \equiv (x|h_\mu)_j \,. \tag{14}$$

Thus, Eq. (9) is rewritten as

$$\ln \Lambda_j = \sum_{\mu=1}^{4} \mathcal{A}_\mu\, x_\mu^{[j]} - \frac{1}{2} \sum_{\mu,\nu=1}^{4} \mathcal{A}_\mu\, \mathcal{M}_{\mu\nu}^{[j]}\, \mathcal{A}_\nu \,. \tag{15}$$

In hierarchical semicoherent searches, for every segment j the log-likelihood ratio (15) is analytically maximized over the amplitude parameters $\mathcal{A}$. The maximum likelihood (ML) estimators for $\mathcal{A}$ obtained from the jth segment are denoted by

$$\hat{\mathcal{A}}^{[j]} = \left(\hat{\mathcal{A}}_1^{[j]}, \hat{\mathcal{A}}_2^{[j]}, \hat{\mathcal{A}}_3^{[j]}, \hat{\mathcal{A}}_4^{[j]} \right) \,, \tag{16}$$

are explicitly given by [19],

$$\hat{\mathcal{A}}_1^{[j]} = 2\, \frac{B_j\, x_1^{[j]} - C_j\, x_2^{[j]}}{D_j} \,, \qquad \hat{\mathcal{A}}_2^{[j]} = 2\, \frac{A_j\, x_2^{[j]} - C_j\, x_1^{[j]}}{D_j} \,,$$

$$\hat{\mathcal{A}}_3^{[j]} = 2\, \frac{B_j\, x_3^{[j]} - C_j\, x_4^{[j]}}{D_j} \,, \qquad \hat{\mathcal{A}}_4^{[j]} = 2\, \frac{A_j\, x_4^{[j]} - C_j\, x_3^{[j]}}{D_j} \,, \tag{17}$$

where $D_j \equiv A_j B_j - C_j^2$, and $D_j \neq 0$ has been assumed.

Replacing the amplitude parameters $\mathcal{A}$ in $\ln \Lambda_j$ of Eq. (15) with their ML estimators $\hat{\mathcal{A}}^{[j]}$ given by Eqs. (17) yields the so-called $\mathcal{F}$-statistic for the jth segment,

$$\mathcal{F}_j \equiv \frac{B_j}{D_j} \left(x_1^{[j]\,2} + x_3^{[j]\,2} \right) + \frac{A_j}{D_j} \left(x_2^{[j]\,2} + x_4^{[j]\,2} \right)$$
$$- \frac{2C_j}{D_j} \left(x_1^{[j]} x_2^{[j]} + x_3^{[j]} x_4^{[j]} \right) \,. \tag{18}$$

This expression can be written compactly by using the four-vector notation for the set of four linear correlations $x_\mu^{[j]}$ as

$$x^{[j]} \equiv (x_1^{[j]}, x_2^{[j]}, x_3^{[j]}, x_4^{[j]}) \,, \tag{19}$$

such that Eq. (18) takes the form

$$\mathcal{F}_j = \frac{1}{2}\, x^{[j]}\, \mathcal{M}^{[j]-1}\, x^{[j]\,\mathrm{T}} \,, \tag{20}$$

where the superscript $^{\mathrm{T}}$ indicates the transpose. Therefore, the $\mathcal{F}$-statistic represents a quadratic form in terms of the linear correlations $x_\mu^{[j]}$. It should be noted that in practice $\mathcal{F}_j$ can be efficiently computed using the FFT algorithm when rewriting the four linear correlations $x_\mu^{[j]}$ as two complex integrals, further details are described in [19, 22].

We find that the $\mathcal{F}$-statistic can equivalently be formulated as a quadratic form in terms of the ML estimators $\hat{\mathcal{A}}_\mu^{[j]}$. Using Eqs. (17) to substitute the $x_\mu^{[j]}$ in Eq. (18) yields

$$\mathcal{F}_j = \frac{A_j}{4} \left(\hat{\mathcal{A}}_1^{[j]\,2} + \hat{\mathcal{A}}_3^{[j]\,2} \right) + \frac{B_j}{4} \left(\hat{\mathcal{A}}_2^{[j]\,2} + \hat{\mathcal{A}}_4^{[j]\,2} \right)$$
$$+ \frac{C_j}{2} \left(\hat{\mathcal{A}}_1 \hat{\mathcal{A}}_2 + \hat{\mathcal{A}}_3 \hat{\mathcal{A}}_4 \right) \,, \tag{21}$$

which is compactly rewritten as

$$\mathcal{F}_j = \frac{1}{2} \hat{\mathcal{A}}^{[j]} \mathcal{M}^{[j]} \hat{\mathcal{A}}^{[j]\mathrm{T}} , \qquad (22)$$

showing that the $\mathcal{F}$-statistic can also be viewed as quadratic form in terms of the $\hat{\mathcal{A}}_\mu^{[j]}$ with a coefficient matrix being equal to $\mathcal{M}^{[j]}$. This formulation (22) of the $\mathcal{F}$-statistic is not common in the existing literature, but closely related is the work of [38–40]. There, the matrix $\mathcal{M}^{[j]}$ is considered as a metric on the amplitude parameter space $\mathcal{A}$ and a norm of the four-vector $\mathcal{A}$ is defined by $||\mathcal{A}|| \equiv \sqrt{\mathcal{A}\,\mathcal{M}^{[j]}\,\mathcal{A}^{\mathrm{T}}}$. In this context, we see from Eq. (22) that the $\mathcal{F}$-statistic is simply half the squared "length" of the four-vector $\hat{\mathcal{A}}^{[j]}$ of amplitude ML estimators: $\mathcal{F}_j = ||\hat{\mathcal{A}}^{[j]}||^2/2$.

2. Statistical properties

The four linear correlations $x_\mu^{[j]}$ for a given segment j are Gaussian distributed random variables, whose expectation values and variances, respectively, are in absence of a signal, when $x(t) = n(t)$, obtained as

$$E_n\left[x_\mu^{[j]}\right] = 0 , \qquad E_n\left[x_\mu^{[j]} x_\nu^{[j]}\right] = \mathcal{M}_{\mu\nu}^{[j]} . \qquad (23)$$

Therefore, in this case the probability density function of $2\mathcal{F}_j$ is a central χ^2 distribution with four degrees of freedom [19]. Hence $2\mathcal{F}_j$ has the following expectation value and variance, respectively,

$$E_n\left[2\mathcal{F}_j\right] = 4 , \qquad \sigma_{2\mathcal{F}_j,n}^2 = 8 . \qquad (24)$$

When a signal is present, which perfectly matches the template waveform $h(t)$, then the expectation values corresponding to Eqs. (23) are obtained as

$$E_h\left[x_\mu^{[j]}\right] = (h|h_\mu)_j , \qquad (25)$$

$$E_h\left[x_\mu^{[j]} x_\nu^{[j]}\right] = \mathcal{M}_{\mu\nu}^{[j]} + (h|h_\mu)_j\,(h|h_\nu)_j . \qquad (26)$$

Thus, as first noted in [19] the covariance matrix for the Gaussian random variables $x_\mu^{[j]}$ is the *same* whether a signal is present or not, and it is exactly equal to $\mathcal{M}^{[j]}$. It should also be noted that the inverse of $\mathcal{M}^{[j]}$ is equal to the covariance matrix of the ML estimators $\hat{\mathcal{A}}_\mu^{[j]}$. Thus in this case $2\mathcal{F}_j$ has noncentral χ^2 distribution with four degrees of freedom and a noncentrality parameter $\rho_j^2 \equiv (h|h)_j$, where ρ_j is commonly referred to as the "optimal signal-to-noise ratio" (S/N). Thus, the expectation value and variance of $2\mathcal{F}_j$ in this perfect-match case are

$$E_h\left[2\mathcal{F}_j\right] = 4 + \rho_j^2 , \qquad \sigma_{2\mathcal{F}_j,h}^2 = 8 + 4\rho_j^2 , \qquad (27)$$

where ρ_j^2 is explicitly obtained as

$$\rho_j^2 = A_j\,\frac{\mathcal{A}_1^2 + \mathcal{A}_3^2}{2} + B_j\,\frac{\mathcal{A}_2^2 + \mathcal{A}_4^2}{2} + C_j\,(\mathcal{A}_1\mathcal{A}_2 + \mathcal{A}_3\mathcal{A}_4)$$
$$= \mathcal{A}\,\mathcal{M}^{[j]}\,\mathcal{A}^{\mathrm{T}} , \qquad (28)$$

with $\mathcal{A}$ representing the 4-vector of the signal's amplitude parameters, $\mathcal{A} = (\mathcal{A}_1, \mathcal{A}_2, \mathcal{A}_3, \mathcal{A}_4)$.

B. Incoherent combination of coherently analyzed segments

1. The standard semicoherent detection statistic

In existing hierarchical CW search methods the standard semicoherent detection statistic computed [24, 28, 35] at a given fine-grid point in phase parameter space is the sum of one $\mathcal{F}$-statistic value $\mathcal{F}_j$ from each segment j, which will be denoted here by $\bar{\mathcal{F}}$ as

$$\bar{\mathcal{F}} = \sum_{j=1}^N \mathcal{F}_j = \frac{1}{2} \sum_{j=1}^N x^{[j]}\,\mathcal{M}^{[j]-1}\,x^{[j]\mathrm{T}} . \qquad (29)$$

Therefore, $\bar{\mathcal{F}}$ also represents a quadratic form in terms of the linear correlations $x_\mu^{[j]}$ and one can compactly rewrite Eq. (29) as

$$\bar{\mathcal{F}} = \frac{1}{2} x\,\bar{\mathcal{M}}^{-1}\,x^{\mathrm{T}} , \qquad (30)$$

where the $4N$-vector x collects all the $x^{[j]}$ as

$$x = (\,x^{[1]}, x^{[2]}, ..., x^{[N]}\,) . \qquad (31)$$

and the $4N \times 4N$ matrix $\bar{\mathcal{M}}$ is defined to have the form

$$\bar{\mathcal{M}} = \begin{pmatrix} \mathcal{M}^{[1]} & & & \\ & \mathcal{M}^{[2]} & & \\ & & \ddots & \\ & & & \mathcal{M}^{[N]} \end{pmatrix} . \qquad (32)$$

Hence, the standard hierarchical detection statistic $\bar{\mathcal{F}}$ represents the incoherent combination of *epochwise* coherent matched-filter outputs, where each epoch has duration T. Recall that using Eq. (22), $\bar{\mathcal{F}}$ can equivalently be rewritten as a quadratic form in terms of the amplitude ML estimators $\hat{\mathcal{A}}^{[j]}$, leading to

$$\bar{\mathcal{F}} = \frac{1}{2} \sum_{j=1}^N \hat{\mathcal{A}}^{[j]}\,\mathcal{M}^{[j]}\,\hat{\mathcal{A}}^{[j]\mathrm{T}} = \frac{1}{2} \hat{\mathcal{A}}\,\bar{\mathcal{M}}\,\hat{\mathcal{A}}^{\mathrm{T}} , \qquad (33)$$

where $\hat{\mathcal{A}}$ denotes the $4N$-vector $\hat{\mathcal{A}} = (\,\hat{\mathcal{A}}^{[1]}, \hat{\mathcal{A}}^{[2]}, ..., \hat{\mathcal{A}}^{[N]}\,)$.

The problem of efficiently selecting the best coarse-grid $\mathcal{F}_j$ value in every segment for a given fine-grid point has been studied in previous work [28, 35] and hence for rest of this paper it is assumed that such an efficient link between the coarse and fine grids is available.

2. Statistical properties

In absence of a signal, it is straightforward to show that the probability density function of $2\bar{\mathcal{F}}$ is a central χ^2 distribution with $4N$ degrees of freedom [24, 37], hence $\bar{\mathcal{F}}$ has expectation value and variance, respectively,

$$E_n\left[2\bar{\mathcal{F}}\right] = 4N , \qquad \sigma_{2\bar{\mathcal{F}},n}^2 = 8N . \qquad (34)$$

On the other hand, if a signal $h(t)$ is present, perfectly matching the template-waveform phase parameters, then $\bar{\mathcal{F}}$ has non-central χ^2 distribution with $4N$ degrees of freedom and non-centrality parameter $\bar{\rho}^2$. The expectation value and variance of $\bar{\mathcal{F}}$, respectively, are obtained as

$$E_h\left[2\bar{\mathcal{F}}\right] = 4N + \bar{\rho}^2 , \qquad \sigma^2_{2\bar{\mathcal{F}},h} = 8N + 4\bar{\rho}^2 , \qquad (35)$$

where $\bar{\rho}$ is given by

$$\bar{\rho}^2 \equiv \sum_{j=1}^{N} \rho_j^2 , \qquad (36)$$

recalling that ρ_j as of Eq. (28) denotes the optimal S/N for the jth segment.

It is interesting to note that $\bar{\rho}$ of Eq. (36) is actually *equal* to the fully-coherent optimal S/N for the entire data set. The apparent difference in search sensitivity results from the different underlying probability distributions. In the standard hierarchical semicoherent scheme there are N times as many degrees of freedom as compared to the fully-coherent case.

IV. SLIDING COHERENCE WINDOW APPROACH

The central idea behind the sliding coherence window scheme is to use a window of size the coherence time baseline T and "slide" it over the data set in steps *smaller* than T to combine the coherent matched-filter outputs from each sliding step. This effectively amounts to the incoherent combination of coherent matched-filter outputs from *overlapping* segments of length T, which remarkably improves the search sensitivity compared to the standard hierarchical scheme. There, only coherent matched-filter outputs from *non-overlapping* segments of coherence length T are combined, omitting to coherently correlate large parts of the data which still lie *within* the coherence time baseline T, as illustrated in Fig. 1.

The number of templates to discretely cover the phase parameter space searched is of great importance, since this is what ultimately limits the overall search sensitivity at the finite computing power available. Therefore, it should also be emphasized that the sliding coherence window technique employs the *same* the number of templates in phase parameter space as the standard scheme. The combination of overlapping coherent integrations, does neither alter the coherence time baseline T nor the total data time span T_{data}. Hence, it is obvious that the same semicoherent metric as previously studied in [28, 35] can also be used in combination with the here proposed sliding coherence window technique [53].

A. Detection statistic

For computational efficiency the sliding coherence window approach subdivides of every segment into q "subsegments", as adumbrated in Fig. 1. Each subsegment is of duration $T_q = T/q$, which represents the step size between each sliding iteration of the coherence window. This way of subdivision
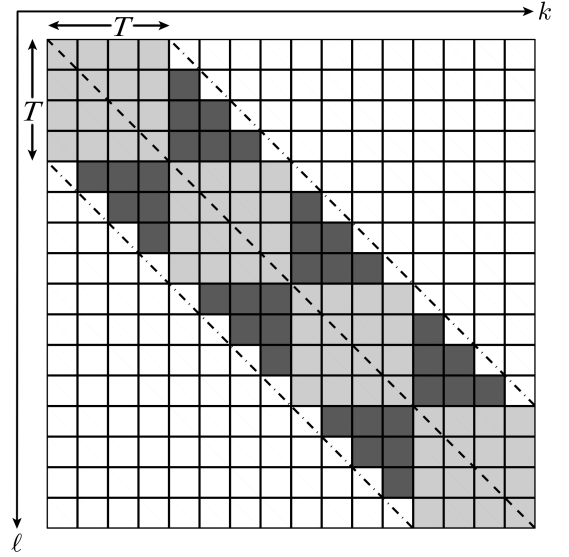

FIG. 1: Schematic comparison of standard hierarchical search scheme and sliding coherence window approach for the same coherence time baseline T. Each box represents one product of the linear correlations $x_\mu^{[k]} x_\mu^{[\ell]}$, obtained from the subsegment k and ℓ, respectively. In this example, the indices take the values $k, \ell = 1, ..., 16$. The light grey colored boxes represent the set of products selected in the standard hierarchical search scheme, for $N = 4$ coherent segments of duration T. The dark grey colored boxes are the *additionally* selected products by the sliding coherence window technique to enhance the search sensitivity. In this example, T is subdivided into $q = 4$ subsegments (implying $\eta = 75\%$ coherence overlap between successive sliding steps). In contrast, a fully-coherent search over the entire data set would have to include all boxes shown.

essentially ensures the avoidance of redundant computation at the coherent stage if $q > 1$. It is obvious that for $q = 1$ the standard hierarchical search method is to be retrieved.

The subsegments are labeled by $k = 1, ..., qN$. Thus, in analogy to Eq. (19) we define the four-vector $x^{[k]}$ for the kth subsegment as $x^{[k]} = (x_1^{[k]}, x_2^{[k]}, x_3^{[k]}, x_4^{[k]})$. In this context, similarly to Eq. (31), the $4qN$-vector now collects all the $x^{[k]}$, $x = (x^{[1]}, x^{[2]}, ..., x^{[qN]})$. Analogously, the same notation also applies to the $4qN$ amplitude ML estimators $\hat{\mathcal{A}}_\mu^{[k]}$.

As sketched in Fig. 1, the central goal of the sliding coherence window strategy is to combine a larger number of *distinct* pairs [54] $\{x_\mu^{[k]}, x_\nu^{[\ell]}\}$, while still restricting the maximum difference between their time stamps t_k and t_ℓ to at most the coherent time baseline T. Hence, the resulting selection condition is $|t_k - t_\ell| \leq T$.

To achieve this goal, in principle an appropriate $4qN \times 4qN$ coefficient matrix $\mathcal{U}$ needs to be constructed, constituting the following quadratic form $\mathcal{Z}$,

$$\mathcal{Z} = \frac{1}{2} x \, \mathcal{U} \, x^{\text{T}} , \qquad (37)$$

which represents the semicoherent detection statistic of the sliding coherence window search technique.

In order to simplify the construction of $\mathcal{U}$, we exploit the fact that the constants C_k are typically much smaller than the

values of A_k and B_k, and therefore terms involving C_k are neglected [55]. With this approximation, Eq. (37) should explicitly read as

$$\mathcal{Z} = \sum_{k,\ell=1}^{qN} Q(t_k - t_\ell) \left[\frac{x_1^{[k]} x_1^{[\ell]} + x_3^{[k]} x_3^{[\ell]}}{\sqrt{A_k\,A_\ell}} + \frac{x_2^{[k]} x_2^{[\ell]} + x_4^{[k]} x_4^{[\ell]}}{\sqrt{B_k\,B_\ell}} \right],$$

(38)

where the step function $Q(t_k - t_\ell)$ selects the pairs of linear correlations according to their time difference and the predefined coherent time baseline T,

$$Q(\Delta t) \equiv \begin{cases} 1 & |\Delta t| \le T \\ 0 & |\Delta t| > T \end{cases} .$$

(39)

As with $\bar{\mathcal{F}}$, the detection statistic $\mathcal{Z}$ can also be equivalently reformulated as a quadratic form in terms of the amplitude ML estimators $\hat{\mathcal{A}}_\mu^{[k]}$. For practical convenience, in what follows we use the $x_\mu^{[k]}$ as in Eq. (38). However, note that in the above approximative case $x_\mu^{[k]} \propto \hat{\mathcal{A}}_\mu^{[k]}$, thus making the interchange between $x_\mu^{[k]}$ and $\hat{\mathcal{A}}_\mu^{[k]}$ simple if desired.

When $q = 1$, it is obvious that $\mathcal{Z}$ coincides with the standard hierarchical detection statistic $\bar{\mathcal{F}}$, as was premised. However, if one chooses $q > 1$, the detection statistic $\mathcal{Z}$ is able to improve performance compared to $\bar{\mathcal{F}}$, as will be described in what follows.

Moreover, a useful quantity is denoted by η, which defines the average "coherence overlap" between successive sliding steps. For the case of a contiguous data set [56], as considered here, η is related to q simply via $\eta = 1 - 1/q$.

B. Statistical properties and sensitivity estimation

To analytically estimate the sensitivity of the sliding coherence window search, the underlying statistical properties are examined. Recall that for simplicity the data set has been taken as free of gaps, such that one can write the time span of the entire data set as $T_{\text{data}} = NT = qN\,T_q$. The detection statistic $\mathcal{Z}$ of Eq. (38) is explicitly written as

$$\mathcal{Z} = \sum_{k=1}^{qN} \left\{ \frac{x_1^{[k]^2} + x_3^{[k]^2}}{A_k} + \frac{x_2^{[k]^2} + x_4^{[k]^2}}{B_k} \right.$$
$$\left. + 2 \sum_{\ell=k+1}^{k+q-1} \left[\frac{x_1^{[k]} x_1^{[\ell]} + x_3^{[k]} x_3^{[\ell]}}{\sqrt{A_k A_\ell}} + \frac{x_2^{[k]} x_2^{[\ell]} + x_4^{[k]} x_4^{[\ell]}}{\sqrt{B_k B_\ell}} \right] \right\}.$$

(40)

Since the actual probability density function $\mathcal{Z}$ is cumbersome to work with, we approximate it here by a Gaussian distribution, which is well justified based on the generalized central limit theorem (provided $N \gg 1$), as done similarly in previous work [25, 26]. Thus, we proceed by computing the mean and variance of $\mathcal{Z}$.

When the data consists of zero-mean stationary Gaussian noise only, the expectation value of $2\mathcal{Z}$ is obtained as

$$E_n[2\mathcal{Z}] = 4qN,$$

(41)

and the variance of $2\mathcal{Z}$ is given by

$$\sigma_{2\mathcal{Z},n}^2 = 8qN(2q - 1).$$

(42)

It is straightforward to show that for Gaussian noise, a certain false alarm probability P_{FA} corresponds to a threshold $\mathcal{Z}_{\text{th}}$ via

$$\mathcal{Z}_{\text{th}} = E_n[\mathcal{Z}] + \sigma_{\mathcal{Z},n}\sqrt{2}\,\text{erfc}^{-1}(2P_{\text{FA}}),$$

(43)

where erfc denotes the complementary error function.

Provided the presence of a signal $h(t)$ whose phase parameters perfectly match the template, then the expectation value of $2\mathcal{Z}$ is given by

$$E_h[2\mathcal{Z}] = 4qN + \rho_{\mathcal{Z}}^2,$$

(44)

where we defined $\rho_{\mathcal{Z}}$ as

$$\rho_{\mathcal{Z}}^2 \equiv \frac{\mathcal{A}_1^2 + \mathcal{A}_3^2}{2} \left\{ \sum_{k=1}^{qN} \left[A_k + 2 \sum_{\ell=k+1}^{k+q-1} \sqrt{A_k A_\ell} \right] \right\}$$
$$+ \frac{\mathcal{A}_2^2 + \mathcal{A}_4^2}{2} \left\{ \sum_{k=1}^{qN} \left[B_k + 2 \sum_{\ell=k+1}^{k+q-1} \sqrt{B_k B_\ell} \right] \right\}. \quad (45)$$

The probability of detection P_{DET} for Gaussian noise is given by

$$P_{\text{DET}} = \frac{1}{2}\,\text{erfc}\left(\frac{\mathcal{Z}_{\text{th}} - E_h[\mathcal{Z}]}{\sqrt{2}\,\sigma_{\mathcal{Z},h}} \right),$$

(46)

For current ground-based detectors, the expected CW signals are extremely weak, so that the small-signal situation ($h \ll n$) well applies. Thus, we approximate $\sigma_{\mathcal{Z},h}$ by using $\sigma_{\mathcal{Z},n}$ and by means of Eqs. (41) - (44) one obtains from Eq. (46) the following relation

$$\rho_{\mathcal{Z}}^2 = \mathcal{E}\sqrt{2}\,\sigma_{\mathcal{Z},n}.$$

(47)

where the constant $\mathcal{E}$ has been defined as

$$\mathcal{E} \equiv \text{erfc}^{-1}(2P_{\text{FA}}) - \text{erfc}^{-1}(2P_{\text{DET}}).$$

(48)

The minimum detectable gravitational-wave strain tensor amplitude h_0 can be determined from Eq. (47), because $h_0^2 \propto \rho_{\mathcal{Z}}^2$ as follows from Eq. (45).

To obtain the estimated sensitivity scaling of the sliding coherence window search from in terms of the most relevant parameters, the noise floor S_n is taken as constant throughout the data set. In addition, we replace the constants A_k and B_k by effective average values as $A_k \approx \frac{2T_q}{S_n} \bar{A}$, and $B_k \approx \frac{2T_q}{S_n} \bar{B}$, and define $\bar{\kappa}$ as

$$\bar{\kappa} \equiv \bar{A}\left(\bar{\mathcal{A}}_1^2 + \bar{\mathcal{A}}_3^2\right) + \bar{B}\left(\bar{\mathcal{A}}_2^2 + \bar{\mathcal{A}}_4^2\right),$$

(49)

where the $\bar{\mathcal{A}}_\mu$ are the same as the $\mathcal{A}_\mu$ apart from the factor h_0, $\bar{\mathcal{A}}_\mu \equiv \mathcal{A}_\mu / h_0$. Thus, Eq. (45) simplifies to

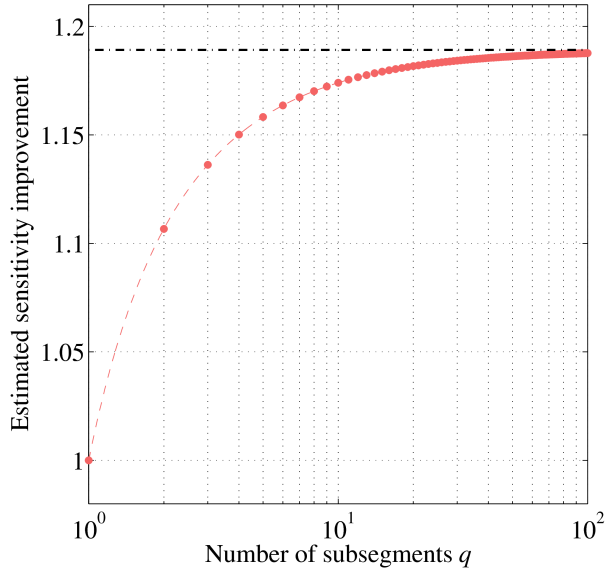$$\rho_{\mathcal{Z}}^2 = h_0^2\,\bar{\kappa}\,\frac{T}{S_n} N\,(2q - 1).$$

(50)

6

FIG. 2: Estimated sensitivity improvement factor of the sliding coherence window technique over the standard hierarchical search strategy, shown as a function of q (number of subsegments). The curve is explicitly given by $(2 - 1/q)^{1/4}$. The horizontal dashed-dotted line indicates the constant value $2^{1/4} \approx 1.19$.

In turn using this relation to substitute $\rho_{\mathcal{Z}}^2$ in Eq. (47) and solving for h_0 yields

$$
h_0 = \frac{2\sqrt{\mathcal{E}}}{\sqrt{\bar{\kappa}}} \sqrt{\frac{S_n}{T}} \, N^{-1/4} \left(2 - \frac{1}{q}\right)^{-1/4} , \qquad (51)
$$

revealing the estimated sensitivity scaling of the sliding coherence window search. One may further rewrite Eq. (51) as

$$
h_0 = \frac{2\sqrt{\mathcal{E}}}{\sqrt{\bar{\kappa}}} \sqrt{\frac{S_n}{T}} \, [N \, (1 + \eta)]^{-1/4} , \qquad (52)
$$

using the previously introduced average coherence overlap η.

C. Comparison of sensitivity with standard scheme

Equation (52) also reveals the estimated sensitivity improvement of the sliding coherence window technique compared to the standard hierarchical search under the same assumptions. The standard hierarchical scheme is recovered for $\eta = 0$ (i.e. $q = 1$), which also yields in agreement with Eq. (36) the S/N as $\bar{\rho}^2 = h_0^2 \, \bar{\kappa} \, N \, T/S_n$. Hence, the sliding coherence window approach is more sensitive than the standard hierarchical search scheme by the factor $(1 + \eta)^{1/4}$. Thus in terms of q the improvement factor is $(2 - 1/q)^{1/4}$, which is shown in Fig. 2. Therefore, it is apparent that the coherence overlap η enhances the search sensitivity effectively as if increasing the number of segments in the standard method. In other words, to achieve the same sensitivity as with the sliding coherence window technique at given T, using the standard hierarchical search method, effectively $1 + \eta$ more segments have to be analyzed (hence $50\,\% - 100\,\%$ more data).

Besides, one might also think of different sliding scheme, in which qN values of $\mathcal{F}$ are summed, that are each computed over an interval of length T, but where the interval boundaries are shifted by T_q at each iterating step. However, such a scheme would be very inefficient since it involves a significant fraction of redundant computation as mentioned earlier. Apart from that, this approach is also in a sense statistically unfavorable, leading to a lower search sensitivity, because of giving too much weight to the "auto-correlation" pairs $\{x_\mu^{[k]}, x_\mu^{[k]}\}$. This observation is also numerically verified as shown by Fig. 3 in the following section.

V. SENSITIVITY PERFORMANCE DEMONSTRATION

The performance improvement of the sliding coherence window technique is demonstrated through realistic Monte Carlo simulations. In particular, ROC (receiver operating characteristic) curves are obtained to compare the standard hierarchical search scheme that is $q = 1$ (corresponding to $\eta = 0$) and the sliding coherence window strategy for $q = 2$ (corresponding to $\eta = 50\%$).

The simulated data set refers to the two LIGO 4-km detectors (H1 and L1) and spans a time interval of $5\,000\,\text{h}$. The coherent time baseline is chosen as $T = 50\,\text{h}$ and thus $N = 100$. The software tools used are part of LALApps [41] and employ accurate barycentering routines with timing errors below $3\mu\text{s}$.

In this study, the phase parameter space considered is four-dimensional using one spindown parameter, as in current all-sky surveys for prior unknown CW sources [12–14]. Thus a point in phase parameter space is labeled by $\mathbf{p} = (f, \dot{f}, \alpha, \delta)$.

The false alarm probabilities are found from thousands of different realizations of stationary Gaussian white noise with $\sqrt{S_n} = 3.25 \times 10^{-22}\,\text{Hz}^{-1/2}$. To obtain the detection probabilities, distinct CW signals with fixed gravitational-wave strain tensor amplitude of $h_0 = 1.0 \times 10^{-24}$ are added. The remaining parameters of the signal population are randomly drawn from uniform distributions in ψ, $\cos\iota$, Φ_0, in the entire sky, frequencies in the interval $f \in [155.12, 155.16]\,\text{Hz}$ and spindowns over the range of $\dot{f} \in [-2.64, 0.264]\,\text{nHz/s}$.

Figure 3 compares the resulting ROC curves for the different search techniques. The ROC curves are computed from $6\,000$ different realizations. The 1σ errors shown in Fig. 3 are based on a jackknife estimate as in [42, 43] using 100 subsets. As expected, the sliding coherence window technique with $q = 2$ is substantially more "powerful" than the standard scheme (retrieved for $q = 1$), yielding a higher probability of detection for the same false alarm probability.

For further comparison, in Fig. 3 a third ROC curve is given, corresponding to summing actual $\mathcal{F}$-statistics computed from 50%-overlapping segments of length T. As explained in Sec. IV C, compared to the sliding coherence window approach this strategy not only involves much more redundant computation, but is also less sensitive as shown in Fig. 3.
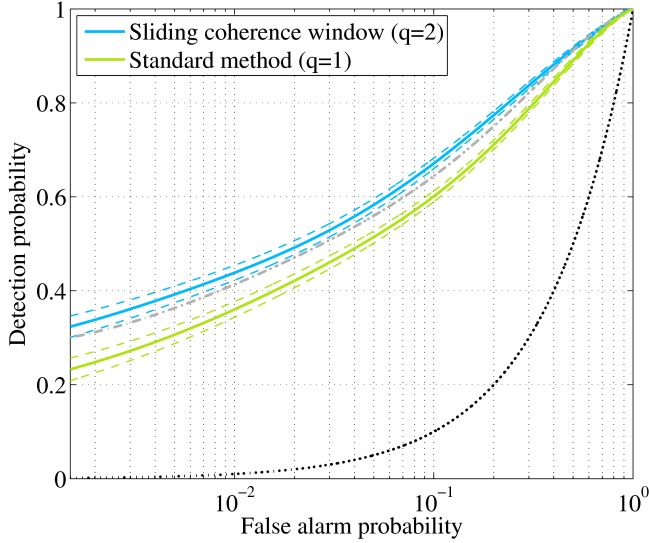
7

FIG. 3: ROC curves for a fixed gravitational-wave amplitude of $h_0 = 1.0 \times 10^{-24}$, comparing the standard hierarchical search technique (30) ($q = 1$) and the sliding coherence window method (38) with $q = 2$ (implying a coherence overlap of $\eta = 50\%$). The dashed curves on either side represent estimated 1σ errors. For comparison, the grey dashed-dotted ROC curve corresponds to actually summing $\mathcal{F}$ values computed from 50%-overlapping segments of length the same coherence time baseline. The black dotted curve is the so-called line of no-discrimination.

VI. COMPARISON AT FIXED COMPUTING COST

In Sec. IV B, Eq. (51) presented the sensitivity estimate of the sliding coherence window technique for a given (finite) amount of data, disregarding aspects of computational cost and essentially assuming unlimited computing power available. The present section investigates the contrary case, finding the amount of data which can be analyzed at limited (fixed) computational resources and a given (fixed) coherence time baseline T.

The computing cost $\zeta^{(1)}$ of a standard two-stage hierarchical search per a certain volume of phase parameter space searched can always be written as a sum in terms of implementation-specific constants ζ_{COH} and ζ_{INCOH} pertaining to the coherent and incoherent combination stage, respectively, as

$$\zeta^{(1)} = \left(\zeta_{\mathrm{COH}} + \zeta_{\mathrm{INCOH}}\, \gamma^{(1)} \right) N^{(1)} , \qquad (53)$$

where $\gamma^{(1)}$ denotes the so-called refinement factor [35] of the incoherent combination stage, and $N^{(1)}$ are the number of segments coherently analyzed.

The computational cost $\zeta^{(q)}$ of the sliding coherence window technique involves q times more summations at the incoherent combination stage, thus

$$\zeta^{(q)} = \left(\zeta_{\mathrm{COH}} + \zeta_{\mathrm{INCOH}}\, \gamma^{(q)}\, q \right) N^{(q)} . \qquad (54)$$

Thus, the total amount of data which can be analyzed at the fixed computational expense using the standard hierar-

chical search scheme is taken as $T_{\mathrm{data}}^{(1)} = T\, N^{(1)}$. In analogy, the amount of data that can be searched at given computing cost using the sliding coherence window approach is $T_{\mathrm{data}}^{(q)} = T\, N^{(q)}$, for the same coherent time baseline T.

The sensitivity of the standard hierarchical search scheme follows $h_0^{(1)} \propto (T_{\mathrm{data}}^{(1)}\, T)^{-1/4}$. Accordingly, the sensitivity of the sliding coherence window technique given in Eq. (51) scales as $h_0^{(q)} \propto (T_{\mathrm{data}}^{(q)}\, T)^{-1/4}\, (2 - 1/q)^{-1/4}$. Thus, we define the sensitivity ratio by $r \equiv h_0^{(1)}/h_0^{(q)}$, which takes the form

$$r = \left(\frac{T_{\mathrm{data}}^{(q)}}{T_{\mathrm{data}}^{(1)}} \right)^{1/4} \left(2 - \frac{1}{q} \right)^{1/4} . \qquad (55)$$

At equal total computing cost, $\zeta^{(q)} = \zeta^{(1)} = \zeta$, inverting Eqs. (53) and (54) for $T_{\mathrm{data}}^{(1)}$ and $T_{\mathrm{data}}^{(q)}$, respectively, one obtains

$$r = \left(\frac{2}{q} - \frac{1}{q^2} \right)^{1/4} \left(\frac{\sqrt{1 + 4q\theta} - 1}{\sqrt{1 + 4\theta} - 1} \right)^{1/4} , \qquad (56)$$

where the constant θ has been defined as

$$\theta \equiv \frac{\zeta\, \zeta_{\mathrm{INCOH}}}{\zeta_{\mathrm{COH}}^2} , \qquad (57)$$

and the refinement factors have been approximated by $\gamma^{(q)} \approx N^{(q)}$, assuming the search includes at most one spin-down parameter (cf. Ref. [35]).

Figure 4 illustrates the sensitivity ratio r of Eq. (56) as a function of θ and for different values of q. It is obvious from Fig. 4, that there are two regimes where r is slowly changing: when θ is either very small or very large. This can be understood as follows. The specific value of θ depends on the code implementation, manifested in the two constants ζ_{COH} and ζ_{INCOH}. Thus, if one constant is much larger than the other, the two different limits can be considered. First, suppose the implementation is such that coherent part (ζ_{COH}) dominates, which implies that θ is very small. Then the sensitivity ratio is described by

$$\lim_{\theta \to 0} r = \left(2 - \frac{1}{q} \right)^{1/4} = (1 + \eta)^{1/4} , \qquad (58)$$

which is the same described by Eq. (52), because the extra computing cost of the sliding coherence window technique is insignificant.

On the other hand, if the incoherent part (measured by ζ_{INCOH}) would be most computational intensive, θ takes a very large value. In this case the sensitivity ratio is described by

$$\lim_{\theta \to \infty} r = \left(2 - \frac{1}{q} \right)^{1/4} q^{-1/8} . \qquad (59)$$

It is also interesting to note that only for $q = 2$, the sensitivity ratio is *always* greater than 1, implying that in this case the sliding coherence window technique should always be more
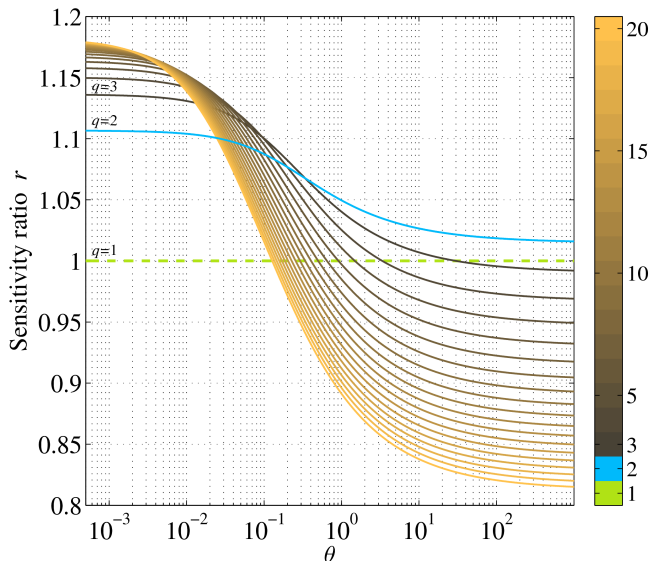
FIG. 4: Estimated sensitivity ratio r (56) of the standard hierarchical search and the sliding coherence window technique at fixed total computational cost and given T, shown as a function of θ (57). The set of different curves correspond to different values of q (number of subsegments) as indicated by the colorbar. The dashed horizontal line corresponds to $q = 1$, for which both search methods are identical.

sensitive than the standard scheme at given T and fixed computational cost.

In the current Einstein@Home [15] analysis, θ is approximately of order 10^{-2}. Thus, the situation in this case rather closer to the regime described by Eq. (58). Hence the Einstein@Home search sensitivity would certainly benefit from employing the sliding coherence window technique.

VII. DISCUSSION

In summary, a novel hierarchical semicoherent strategy to search for prior unknown continuous gravitational-wave sources has been presented, which exploits a sliding coherence window. Standard hierarchical searches divide the data into N non-overlapping segments that are coherently analyzed and subsequently matched-filter outputs are combined incoherently. Thereby, the duration of one segment defines the (maximum) time span of coherence. In contrast, the presented sliding coherence window approach divides each of the N data segments into q subsegments, which are thus *shorter* than the desired maximum coherence length T (size of the coherence window). This permits the efficient combination of matched-filter outputs from all subsegments in a "sliding-window" fashion: If subsegments are closer than T they are combined coherently, otherwise incoherently.

As a result, the estimated search sensitivity of the sliding coherence window approach is considerably superior compared to the standard hierarchical scheme, while using the *same* number of coarse- and fine-grid templates to cover the

parameter space (because the coherence time baseline T is unchanged). At a given value of T, the sensitivity improvement in terms of minimum detectable gravitational-wave amplitude h_0 scales with the fourth root of $N(2 - 1/q)$ for a contiguous data set. Since for the standard hierarchical method $q = 1$, to achieve the same sensitivity as the sliding coherence window technique, between $50\,\% - 100\,\%$ more data (to increase N) would have to be analyzed. Realistic Monte-Carlo simulations have been carried out confirming the sensitivity enhancement.

The sensitivity improvement can also be expressed in terms of the average coherence overlap η between successive sliding steps. In particular if the data set has gaps in time, η is a more useful figure of merit. The sensitivity improvement of the sliding coherence window technique over the standard scheme approximately scales as the fourth root of $(1 + \eta)$.

In addition, the sensitivity has also been compared at fixed computational cost. When the computing cost of the coherent stage dominates the above sensitivity improvement holds. In case, the computational cost of the incoherent stage dominates, the sensitivity improvement can fade away (depending on the search setup). However, it is found (ignoring time gaps in the data set) that when the chosen coherence window is equal to the length of 2 subsegments, the sensitivity is always superior to the standard method at the same estimated computational expense.

It should be mentioned that the proposed approach has similarities with a particular setup of the cross-correlation technique [26] or the "loosely-coherent" method [27]. Both approaches correlate short Fourier-transformed data stretches (SFTs) that have typically a duration of 30 minutes, a time scale during which a CW signal's frequency is expected to remain within one frequency bin. However, at the same coherent time baseline of order days, as considered here, a cross-correlation method might be less computationally efficient, since in hierarchical searches the coherent stage based on input SFTs can be performed by using the FFT algorithm. Which analysis technique is finally most efficient depends on many aspects, such as search parameter space, the input data, code implementation, computational resources available etc. and thus warrants further investigation. Apart from that, Ref. [26] states that the cross-correlation method should be more sensitive than the standard hierarchical scheme when including correlation of SFT pairs from adjacent segments. However, the sliding coherence window approach described here exactly addresses this drawback of the standard hierarchical scheme in a computationally efficient manner to enhance the sensitivity.

However, further topics are planned to be investigated in future work. One of these aspects concerns the efficient implementation the proposed technique, while exploiting the FFT algorithm to perform the sliding combination. Moreover, an optimal weighting scheme between the coherent matched-filter outputs from different subsegments could be further studied, taking into account correlations between these.

The sliding coherence window approach is envisioned to be employed by the Einstein@Home [15] project to further improve the search sensitivity of current all-sky surveys for

unknown isolated CW sources [28]. The proposed approach should also be extensible to CW searches for sources in binary systems [44]. With suitable modification, the method might also have applicability in further related areas, for instance regarding computationally-limited searches for prior unknown radio [45], X-ray [46], and gamma-ray pulsars [47–50].

VIII. ACKNOWLEDGMENTS

[1] B. J. Owen, L. Lindblom, C. Cutler, B. F. Schutz, A. Vecchio, and N. Andersson, Phys. Rev. D **58**, 084020 (1998).

[2] G. Ushomirsky, C. Cutler, and L. Bildsten, Mon. Not. Roy. Astron. Soc. **319**, 902 (2000).

[3] C. Cutler, Phys. Rev. D **66**, 084025 (2002).

[4] D. I. Jones and N. Andersson, Mon. Not. Roy. Astron. Soc. **331**, 203 (2002).

[5] B. J. Owen, Phys. Rev. Lett. **95**, 211101 (2005).

[6] C. J. Horowitz and K. Kadau, Phys. Rev. Lett. **102**, 191102 (2009).

[7] B. Abbott et al. (The LIGO Scientific Collaboration), Rep. Prog. Phys **72**, 076901 (2009).

[8] F. Acernese et al. (The Virgo Scientific Collaboration), Class. Quant. Grav. **23**, 635 (2006).

[9] H. Grote (for the LIGO Scientific Collaboration), Class. Quant. Grav. **25**, 114043 (2008).

[10] R. Takahashi and the TAMA Collaboration, Class. Quant. Grav. **21**, S403 (2004).

[11] B. Abbott et al. (The LIGO Scientific Collaboration), Phys. Rev. D **77**, 022001 (2008).

[12] B. Abbott et al. (The LIGO Scientific Collaboration), Phys. Rev. D **79**, 022001 (2009).

[13] B. Abbott et al. (The LIGO Scientific Collaboration), Phys. Rev. Lett. **102**, 111102 (2009).

[14] B. Abbott et al. (LIGO Scientific Collaboration), Phys. Rev. D **80**, 042003 (2009).

[15] Einstein@Home is available at http://einstein.phys.uwm.edu/.

[16] B. Abbott et al. (The LIGO Scientific Collaboration), Astrophys. J. Lett. **683**, L45 (2008).

[17] J. Abadie et al. (The LIGO Scientific Collaboration), Astrophys. J. **722**, 1504 (2010).

[18] N. Andersson, V. Ferrari, D. I. Jones, K. D. Kokkotas, B. Krishnan, J. S. Read, L. Rezzolla, and B. Zink, arXiv:0912.0384 (2010).

[19] P. Jaranowski, A. Królak, and B. F. Schutz, Phys. Rev. D **58**, 063001 (1998).

[20] C. Cutler and B. F. Schutz, Phys. Rev. D **72**, 063006 (2005).

[21] P. R. Brady, T. Creighton, C. Cutler, and B. F. Schutz, Phys. Rev. D **57**, 2101 (1998).

[22] P. Patel, X. Siemens, R. Dupuis, and J. Betzwieser, Phys. Rev. D **81**, 084032 (2010).

[23] P. R. Brady and T. Creighton, Phys. Rev. D **61**, 082001 (2000).

[24] C. Cutler, I. Gholami, and B. Krishnan, Phys. Rev. D **72**, 042004 (2005).

[25] B. Krishnan, A. M. Sintes, M. A. Papa, B. F. Schutz, S. Frasca, and C. Palomba, Phys. Rev. D **70**, 082001 (2004).

[26] S. Dhurandhar, B. Krishnan, H. Mukhopadhyay, and J. T. Whelan, Phys. Rev. D **77**, 082001 (2008).

[27] V. Dergachev, Class. Quant. Grav. **27**, 205017 (2010).

[28] H. J. Pletsch and B. Allen, Phys. Rev. Lett. **103**, 181102 (2009).

[29] H. J. Pletsch, Phys. Rev. D **78**, 102005 (2008).

[30] R. Prix and Y. Itoh, Class. Quant. Grav. **22**, S1003 (2005).

[31] R. Balasubramanian, B. S. Sathyaprakash, and S. V. Dhurandhar, Phys. Rev. D **53**, 3033 (1996).

[32] B. J. Owen, Phys. Rev. D **53**, 6749 (1996).

[33] I. Jones, B. J. Owen, and D. Whitbeck, LIGO Document T0900500-v1, available at https://dcc.ligo.org/ (2005).

[34] R. Prix, Phys. Rev. D **75**, 023004 (2007).

[35] H. J. Pletsch, Phys. Rev. D **82**, 042002 (2010).

[36] P. Jaranowski and A. Królak, Phys. Rev. D **59**, 063003 (1999).

[37] P. Jaranowski and A. Królak, Phys. Rev. D **61**, 062001 (2000).

[38] R. Prix and J. T. Whelan, Class. Quant. Grav. **24**, 565 (2007).

[39] J. T. Whelan, R. Prix, and D. Khurana, Class. Quant. Grav. **25**, 184029 (2008).

[40] J. T. Whelan, R. Prix, and D. Khurana, Class. Quant. Grav. **27**, 055010 (2010).

[41] http://www.lsc-group.phys.uwm.edu/daswg/.

[42] R. Prix and B. Krishnan, Class. Quant. Grav. **26**, 204013 (2009).

[43] J. H. Conway and N. J. A. Sloane, SIAM J. Algebr. Discrete Methods **5**, 294 (1984).

[44] C. Messenger, LIGO Document P1000020-v1, available at https://dcc.ligo.org/ (2010).

[45] S. M. Ransom, S. S. Eikenberry, and J. Middleditch, Astronom. J. **124**, 1788 (2002).

[46] B. A. Vaughan et al., Astrophys. J. **435**, 362 (1994).

[47] A. M. Chandler, D. T. Koh, R. C. Lamb, D. J. Macomb, J. R. Mattox, T. A. Prince, and P. S. Ray, Astrophys. J. **556**, 59 (2001).

[48] W. B. Atwood, M. Ziegler, R. P. Johnson, and B. M. Baughman, Astrophys. J. Lett. **652**, L49 (2006).

[49] A. A. Abdo et al., Science **325**, 840 (2009).

[50] P. M. Saz Parkinson et al., Astrophys. J. **725**, 571 (2010).

[51] B. Krishnan (private communication).

[52] For simplicity, in this work only a single-detector input data stream is considered. However, it is straightforward to generalize the proposed search technique to multiple-detector input data based on the results of [20, 34].

[53] One may further illustrate this by noting that the semicoherent metric is effectively the "average" of all individual-segment coherent metrics [23, 28, 35]. Thus, in this sense at fixed coherence baseline T and at fixed total data time span T_{data} the

additional overlapping segments do not change the "averaged" metric [51].

[54] Equivalently, one could also employ the pairs $\{\hat{\mathcal{A}}_\mu^{[k]}, \hat{\mathcal{A}}_\nu^{[\ell]}\}$.

[55] The covariance matrix of the Gaussian random variables $x_\mu^{[k]}$ can always be diagonalized via a linear transformation given by Eq.(65) of Ref. [19]. Besides, C_k exactly vanishes when com-

puted over a time interval of a multiple of one sidereal day [37]. Also note that when averaged over all sky positions (α, δ), (in contrast to A_k and B_k) the constant C_k is equal to zero.

[56] When the data contains gaps, the average coherence overlap η is a function of the subsegment time midpoints t_k.